THE INFLUENCE OF TOPOGRAPHY ON THE SPECIFIC DISSIPATED FRICTION POWER IN ULTRA-MILD SLIDING WEAR: EXPERIMENT AND SIMULATION*

Daniel Stickel[1]
Alfons Fischer[2]

Abstract

Current political, economic and ecological guidelines demand the increase of power densities of nearly all machinery parts today. In order to further lower the wear rate towards the ultra-mild sliding wear regime an integral approach is needed, which has to regard contact conditions, surface topography, surface chemistry, as well as sub-surface properties. Still there are no simple parameters to classify the performance of tribosystem. In this study the area and volume affected by tribocontacts are calculated by means of a three dimensional elastic-ideal plastic contact model. The surfaces are generated by means of conventional machining procedures and characterized by scanning white light interferometry. The further input data as to normal and friction forces are derived by ultra-mild sliding wear tests under boundary lubrication conditions of carburized steel against carburized steel and 52100 steel against case-hardened spheroidal cast iron. This contribution will depict the distinct influence of the topography on friction and ultra-mild sliding wear of common Fe-base materials and point on the marked importance of highly localized effects, which govern the acting mechanisms.

Keywords: Ultra-mild sliding wear tests; Carburized steel; Case-hardened spheroidal cast iron; Experiment and simulation.

[1] *Mechanical Engineer/ Dipl.-Ing., Research Assistant, Mechanical Engineering, Chair of Material Science and Engineering, University of Duisburg-Essen, Duisburg, Germany.*
[2] *Mechanical Engineer/ Prof. Dr.-Ing., Mechanical Engineering, Chair of Material Science and Engineering, University of Duisburg-Essen, Duisburg, Germany.*

1 INTRODUCTION

Wear of machinery parts as a result of tribological loads is not inevitable acting throughout the transmission of power by means contacting surface. Even in properly lubricated systems wear occurs e.g. by periods of boundary lubrication during start-up and shut-down sequences. Now modern economic and ecological guidelines demand the increase of the power densities of nearly all machinery parts which can also cause a shift from EHL towards mixed and/or boundary lubricated regimes for the entire operation time. Thus, whenever it comes to design of such machinery parts, the designer has to have knowledge about how much the system will wear over service time e.g. for sizing the parts and schedule the maintenance service. The wear rate for example covers a simple linear relationship between an empirical measured wear depth or wear volume and the sliding distance of a specific system e.g. [1]. Looking at the wear rates of tribosystems over time a running-in and a steady-state wear rate can be distinguished while it might decrease by some orders of magnitude [2]. This effect can be roughly explained by the adaption of the surface topographies of the contacting bodies. Here surface irregularities or roughness summits will be plastically deformed and/or worn off in the running-in phase [3].

Nowadays wear rates are desired to be within the ultra-mild wear regime. This means that the actual wear depth do not exceed the maximum surface roughness for a long period of time. Highly localized effects of the dissipation of friction will have a major influence on the performance of such tribosystem, which still cannot be described by classical wear or statistical surface roughness parameters. To further decrease those wear rates an integral approach is needed, which covers the surface topographies, near surface materials properties and microstructural alterations during tribological loads as well as during the preceding machining processes.

A first step could be to generate optimized contact conditions in order to avoid a distinct running-in phase. Thus in this study two different martensitic materials with similar topographies are analyzed in a boundary lubricated ball-on-plane wear test. One system is a carburized steel running self-mated in gear oil while the other consisted of a 52100 steel ball against case-hardened spheroidal cast iron in motor oil. Two different surfaces were generated by means of standard machining and finishing and by a polishing process. In addition numerical contact simulation is conducted (3D linear elastic-ideally plastic half-space [4, 5]) in order to analyze the real area of contact (affected area) during run-in and steady state. These values were then combined with the measured forces, displacements, and velocities to gain the locally dissipated friction power per contact area. The results are presented and discussed as to the tribological behavior.

2 MATERIAL AND METHODS

The first part of this study covers the conducted wear tests on a custom build tribometer. Here two differing couples consisting of a self-mating carburized steel and a 52100 steel against a case-hardened spheroidal cast iron are subjected to the same nominal tribological load expect that the lubrication was provided by a gear oil (Mobile SHC Gear Oil; $\eta(40°C) = 320$ mm^2/s) for the steel couple and by an engine oil (Mobile 1^{TM} ESP Formula 5W-30; $\eta(40°C) = 72.8$ mm^2/s) for the cast iron at 80°C. Two topographies were chosen for each couple; milled and polished, respectively.

2.1 Carburized Martensitic Steel – 18CrNiMo7-6 (1.6587)

The carburized martensitic steel 18CrNiMo7-6 (Table 1) is used for example in highly stressed gears for wind power plants.

Table 1. Chemical composition of 18CrNiMo7-6

C	Fe	Si max.	Mn	P max.	S	Mo	Ni
0.15..0.21	bal.	0.4	0.5 ..0.90	0.025	0.035	0.25..0.35	1.4 ..1.7

After carburizing the near-surface hardness is 650±30 HV10. Both base and counter bodies were taken from identical blanks. The geometry of the base body is 10x10x15 mm³ (hight x width x depth) while the counterbody is a polished hemisphere with a 5 mm contact radius. Material properties of the bulk material are as follows.

Table 2. Physical properties of 18CrNiMo7-6

Young's Modulus	Possion's ratio	Thermal conductivity	Spec. Heat capacity	Density
210 GPa	0.3	$49.0 \frac{W}{mK}$	$431 \frac{J}{kgK}$	$7770 \frac{kg}{m^3}$

2.2 52100 Steel Balls acc. DIN 5401 / ISO 3290

Standardized 52100 (100Cr6) roller bearing steel balls (Table 3) acc. DIN 5401 / ISO 3290 were used as counterbodies against spheriodal cast iron blocks.

Table 3. Physical properties of 57100

Young's Modulus	Possion's ratio	Thermal conductivity	Spec. Heat capacity	Density
210 GPa	0.3	$42.6 \frac{W}{mK}$	$470 \frac{J}{kgK}$	$7610 \frac{kg}{m^3}$

2.3 Speroidal Cast-Iron EN-GJS-HB 265 (case-hardened)

Spheroidal cast iron (Tables 4 and 5) is a possible alternative to steel and, therefore, used e.g. as crankshafts in combustion engines of cars and trucks [6].

Table 4. Chemical composition of EN-GJS-HB 265

C	Fe	Mg	Mn	Ni	Si
3.3..3.8	bal.	0.02 ..0.07	0.2..0.5	0..1	2..3

After flame hardening the near-surface hardness is 550±30 HV10.

Table 5. Physical properties of 52100

Young's Modulus	Possion's ratio	Thermal conductivity	Spec. Heat capacity	Density
174 GPa	0.275	$32.5 \frac{W}{mK}$	$515 \frac{J}{kgK}$	$7200 \frac{kg}{m^3}$

2.3 Surface Topographies of Base Bodies

Before wear testing the base bodies were processed by milling and polishing. The milling process was carried out by the same milling process parameters for both base body materials on a five-axis machining center [7]. The process parameters are as follows:

Table 6. Milling process parameter

Indexable insert	Cutting speed	Feed per tooth	Cutting depth
TiAlN	$640 \frac{m}{min}$	$0.05 \frac{mm}{z}$	0.2 mm

Polished surfaces were prepared by standard metallographic methods using diamond suspension with a particle size up to 1µm. Figures 1 and 2 are showing the unworn surfaces profiles after milling and polishing.

a)   b)
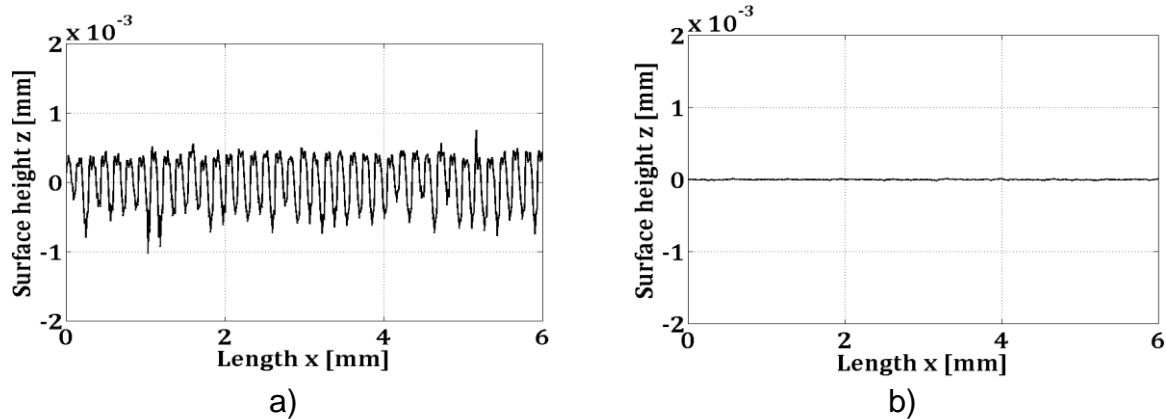
Figure 1. Surface topography of 18CrNiMo7-6 base bodies a) milled surface with an RMS of 0,356 µm b) polished surface with an RMS of 0,0097 µm

a)   b)
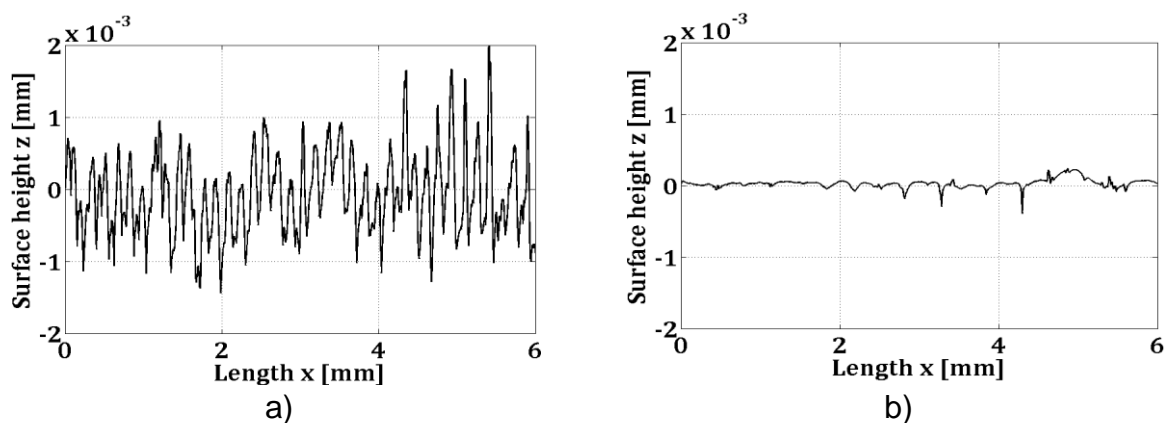
Figure 2. Surface topography of cast iron base bodies a) milled surface with an RMS of 0,551 µm b) polished surface with an RMS of 0,0563 µm

---

* Technical contribution to the 2nd International Brazilian Conference on Tribology – TriboBR 2014, November 3rd to 5th, 2014, Foz do Iguaçu, PR, Brazil.

2.3 Wear tests

All wear test were carried out as reciprocating sliding wear tests (Figure 3; sphere-on-plane) at f_{Test} = 5 Hz, a total stroke length of s = 6 mm and under a normal force of F_N = 30 N. The tangential (friction) force in sliding direction F_{R_y} and that orthogonal to it F_{R_x} were measured by a 3-axis dynamometer (Type 9257A, Kistler Instrumente AG, Winterthur, Switzerland) every 200 cycles (sampling rate = 2048 Hz) over three cycles. Here only F_{R_x} is considered and further mentioned as F_R. In addition the actual displacement was recorded. After predefined test-cycles (75.000, 150.000, 300.000, 600.000, 1.2 Mio and 2.0 Mio) the samples were dismounted and cleaned for 1 min ultrasonically in ethanol. Then the worn surfaces were examined as to the wear appearances by means of confocal white light microscopy (CWLM) (µSurf, Nanofocus, Oberhausen, Germany) as well as light microscopy (LM). The confocal scanning process was done with a lateral resolution of Δx = Δy = 1.5656 µm. Afterwards surface height data were filtered with a software high pass and low pass Gaussian filter with a cutoff-wavelength of $λ_{CH}$ = 25 µm and $λ_{CL}$ = 800 µm, respectively. Two indentations marks outside of the wear scar should allow superimposing the topographies and calculating the worn volume. Special attention was paid to the re-positioning of both samples after each test period in order to avoid or at least minimize the recurrence of any new running-in.

2.4 Numerical Calculations

The numerical calculations include the lubrication regime and the 3D micro contact model. The lubrication is treated as a isothermal elastohydrodynamic lubrication of concentrated contacts according to [8]. The micro contact model is assumed being dry contact based on [4, 9-11]. As a result of the lubrication regime calculation the lambda-ratios [12], the contact area, the dissipated friction power and the contact stress field could be calculated, while the latter is not reported here. Because of the alteration of the surface topography is not known for every test cycle, the numerical contact calculations were performed after each surface topography analysis on the basis of the associated test rig data. Due to the large amount of surface height data (avg. 7000x2500 datapoints) caused by the measurement of the whole body the calculation of the micro contact for every instance was synchronized to the sampling rate of the wear test. As determined by the test frequency, the stroke and the sampling rate there are 205 measured values per half cycle and, therefore, 205 calculations per half cycle. Every time instance will be subscripted by the index i e.g. t_i.
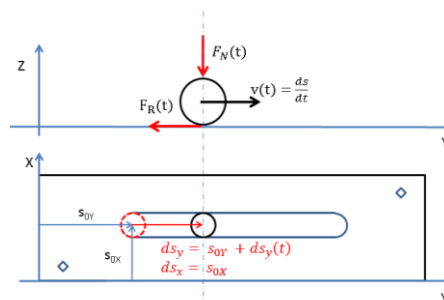
Figure 3. Front and top view of the configuration of contact calculation

2.4.1 Calculation of lubrication regime

The calculation of the lubrication regime is divided into the calculation of the minimum film thickness acc. [8] and the Tallian-Parameter as follows. The minimum film thickness h_{min}:

$$h_{min} = 3.63\ U^{0.68} G^{0.49} W^{-0.073}(1 - e^{-0.68k}) \qquad (1)$$

The viscosity-pressure coefficient and the dynamic viscosity were chosen from oil data sheets.

The Tallian-Parameter was then calculated by

$$\lambda = \frac{h_{min}}{\sqrt{R_{q,1}^2 + R_{q,2}^2}} \qquad (2)$$

with $R_{q,i}$ being the root mean square roughness of the body and counter body in the direction of relative velocity as derived from surface topography measurement.

2.4.2 Calculation of the Real Contact Area (affected Area of Contact)

The calculation of the real contact area was performed using a simplified micro linear elastic – perfectly plastic contact algorithm acc. to [5]. The limiting value for the micro contact pressure is set to the hardness of the softer material. Basically this algorithm computes the pressure distribution without plastic strains and, thus, neglects any residual stresses. The general contact model can be written as a set of equations:

$$F_N = \int_\Omega p(x, y)d\Omega \qquad (3)$$

$$h(x, y) = u_z(x, y) + h_{ini}(x, y) - \delta \geq 0 \qquad (4)$$

$$p(x, y) \geq 0 \ \wedge \ p(x, y) \leq p_{max} \qquad (5)$$

$$h(x, y)p(x, y) = 0 \qquad (6)$$

$$p(x, y) = 0 \ \not\subset \Omega \qquad (7)$$

$$h(x, y) = 0 \ \subset \Omega \qquad (8)$$

With h being the gap between the deformed contact bodies, u_z the normal deflection of both surfaces, h_{ini} the initial gap between the undeformed bodies and δ rigid body approach. Furthermore force balance has to be achieved, pressures within the contact area Ω are nontensile, limited by an upper value and both contacting bodies are impenetrable. In order to calculate the displacement and thus the pressure distribution depending on the load, the gap between the contacting bodies and the material parameters an appropriate calculation domain, which includes the final contact area, has to be established. By doing so the initial gap between both contacting bodies is derived from surface topographies measurements. The relationship between the surface displacement due to normal pressure and traction can be written as [13]:

$u_z(x, y, t_i) = \sum_{n=1}^{N_\Omega} D^n(x - x', y - y')p(x', y', t_i) + \sum_{n=1}^{N_\Omega} D^s(x - x', y - y')\mu(t_i)p(x', y', t_i)$ (9)

The first part accounts for the deflection due to the pressure on top of the surface, the second accounts the deflection due to traction caused by friction.

The set of inequalities (3-8) and equation (9) are solved using a single-loop iterative scheme based on the conjugate gradient method combined with a DC-FFT (Discrete-Convolution Fast Fourier Transform) technique to calculate the displacement u_z [4, 5, 10]. Afterwards the pressure distribution is used to calculate the specific dissipated friction power. The specific dissipated friction power (SPFP) is calculated by

$\dot{E}_{Fric}(x, y, t_i) = \mu(t_i)p(x, y, t_i)v(t_i)$ (10)

The SPFP can be summed up for one half cycle of the wear test over the chosen domain. From this the affected area can be calculated. This is done by counting the calculated SPFP as a frequency of occurrence in discrete and constant intervals. The cumulated frequencies of occurrence are then proportional to the affected area.

3 RESULTS

In context of the wear tests, the measured coefficient of friction and the wear appearances will be presented and discussed first.

3.1 Coefficient of Friction
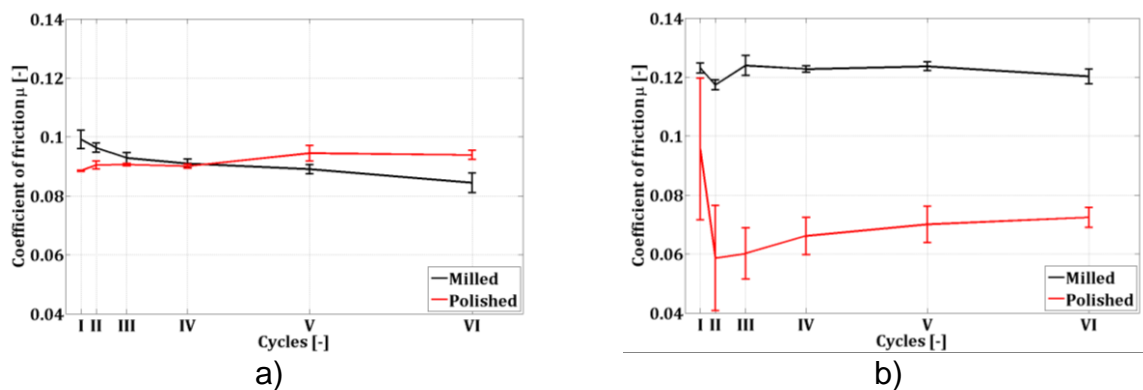
Figure 4. Measured coefficients of friction for a) 18CrNiMo7-6, b) EN-GJS-HB 265

The measured coefficient of friction (CoF) of the conducted wear tests can be seen in Figure 4 a) and b) regarding the 18CrNiMo7-6 and EN-GJS-HB 265 wear tests respectively. Every tested couple was showing a different characteristic over testing time. In case of the milled body of the 18CrNiM07-6 couple the CoF started with a mean value of $\mu \approx 0.1 \pm 0.003$ in the first test interval of 0 – 75000 cycles (denoted as Roman numeral I) and decreases to $\mu \approx 0.084 \pm 0.003$ in the last interval of 1200000 – 2000000 cycles (denoted as Roman numeral VI). In case of the polished body of the 18CrNiMo7-6 couple the CoF started at about $\mu \approx 0.088 \pm 0.0001$ in the first test interval and is then slightly increasing to a value of about $\mu \approx 0.093 \pm 0.001$ at the last interval. The 57100 steel against case-hardened EN-GJS-HB 265 couple showed different CoF characteristics compared to the 18CrNiMo7-6 couple. Here for the milled body the CoF started with a relatively high value of $\mu \approx 0.123 \pm 0.0017$ within the first interval and stabilized in the last test interval at a value of $\mu \approx 0.12 \pm 0.0025$.

In case of the polished body the CoF was starting at a value of µ ≈ 0.09 ± 0.024 in the first interval then decreases to a value of ≈ 0.058 ± 0.0017 in the second interval and then increases slightly up to a value of ≈ 0.072 ± 0.0025.

3.2 Wear Rates after 2 Mio Cycles

After 2 Mio. wear cycles wear loss was so small that it could not be detected by weighting with an accuracy of 10^{-4} g. Thus the worn volume was calculated by the differences of the surfaces profiles of the unworn and worn surfaces. Figures 5 and 6 show such profile differences for 18CrNiMo7-6 and EN-GJS-HB265 for both topographies after 2 Mio cycles.

a)   b)
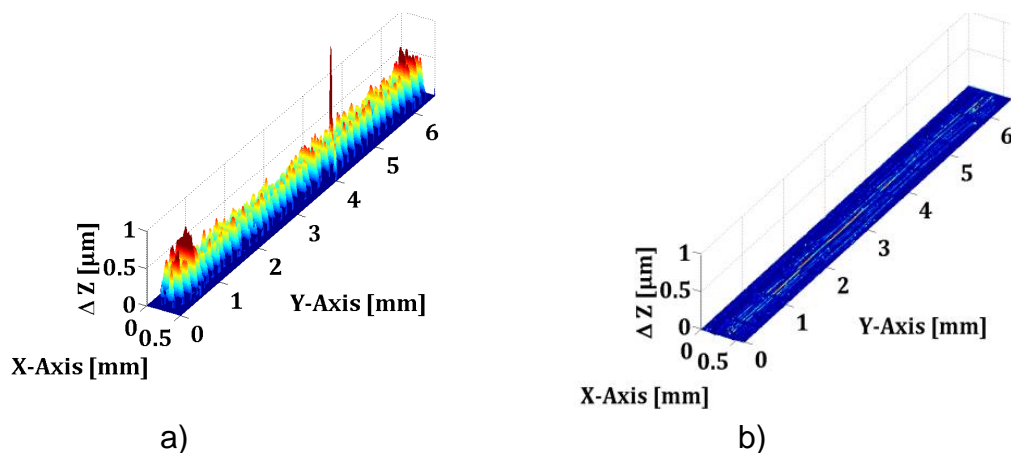
Figure 5. Calculated surface height difference between worn and unworn surfaces a) milled and b) polished base body of 18CrNiMo7-6 samples

a)   b)
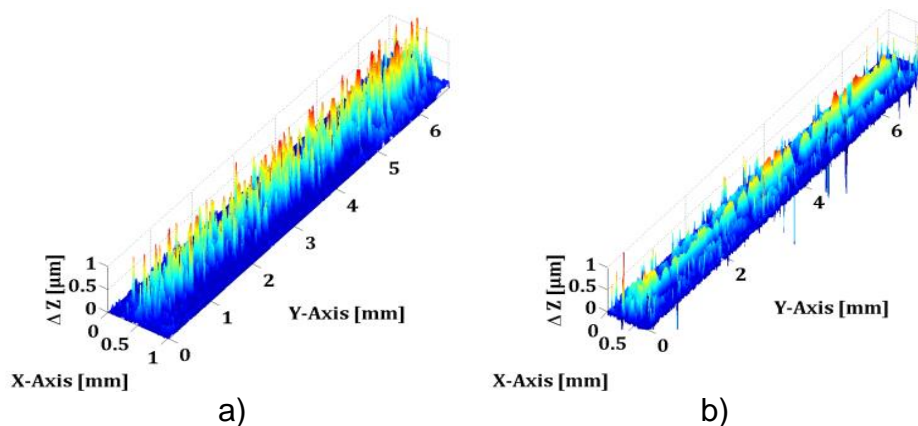
Figure 6. Calculated surface height difference between worn and unworn surfaces a) milled and b) polished base body of iron cast samples

From these measurements and combination with those of the counter bodies one can calculate the wear factor w e.g. acc. to the GfT-standard [14]. By integrating over the profile along the nominal area of the wear scar (1,23 mm^2) and relate that to the wear path one can also gain a characteristic depth in nm/h, as it is usual in automotive industry. Both procedures derive usual factors as shown in Table 7. According to these calculations it can be seen that the polished surface of the 18CrNiMo7-6 showed the least wear compared to the rest. The combined wear volumes of the bodies and counter-bodies and wear rates are:

Table 7: Wear factors

Topography and Material of the Body	Wear Volume after 2×10^6 in μm^3	k-Factor according to [14] in 10^{-10} mm^3/Nm	Wear Factor in nm/h
Milled (18CrNiMo7-6)	507,000	7.04	3.71
Polished (18CrNiMo7-6)	18,100	0.25	0.13
Milled (EN-GJS-HB 265)	1,481,232	20.56	10.8
Polished (EN-GJS-HB 265)	1,507,493	20.94	11.04

Obviously the wear can alter by one order of magnitude depending on the topography while that of the steel couple is smaller than that of the cast iron vs. 52100 steel. The criterion for ultra-mild sliding wear is not standardized yet but is generally set to be less than about 10 nm/h which is fulfilled by all wear tests in table 7.

3.3 Wear Appearances

3.3.1 Milled Topography

a)

b)
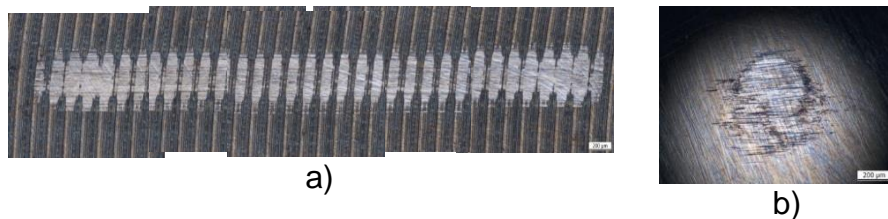
Figure 7. 18CrNiMo7-6; Wear appearances of the a) milled body and b) corresponding counter-body

The wear appearances of the milled body and the corresponding counter-body are shown in Figure 7. Wear appearances can be clearly seen as polished like areas on the body which take place at summits of the machining marks. At both dead centers the wear appearances develop more distinct. The counter-body displays a Hertzian like contact area with scars and scratches.

a)

b)

Figure 8. EN-GJS-HB 265; Wear appearances of the a) milled body and b) corresponding counter-body

Wear appearances of the milled spheroidal cast iron body (Figure 8) is similar to that of the milled 18CrNiMo7-6 body. Still on the counter-body a smoother Hertzian like contact area can be seen.

---

* Technical contribution to the 2nd International Brazilian Conference on Tribology – TriboBR 2014, November 3rd to 5th, 2014, Foz do Iguaçu, PR, Brazil.

3.3.2 Polished Topography

a)

b)
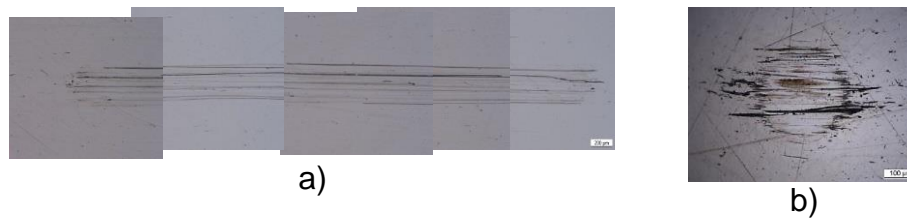
Figure 9. 18CrNiMo7-6; Wear appearances of the a) polished body and b) corresponding counter-body

The wear appearances of the polished body and the corresponding counter-body are shown in Figure 9. Scratches dominate the body while a Hertzian like contact area can be seen on the counter-body again with scars and scratches. Some agglomerated wear products are visible at the boundary of the contact area.

a)

b)
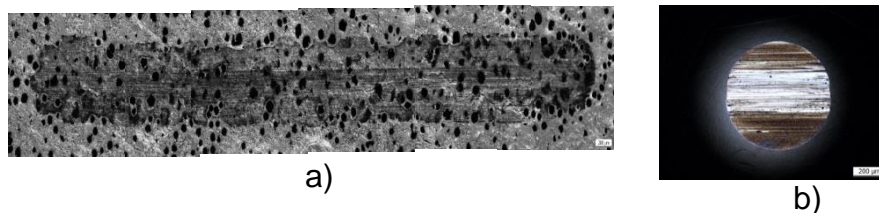
Figure 10. EN-GJS-HB 265; Wear appearances of the a) polished body and b) corresponding counter-body

Wear appearances on the polished cast iron body (Figure 10) reveal a dark surface layer. The counter-body displays a Hertzian like contact area with polished like parts in the center of the contact area surrounded by dark areas.

3.4 Lubrication regime

In case of the Mobile Gear SHC 320 oil lubricant and the 18CrNiMo7-6 wear test at room temperature of 22°C a theoretical minimum film thickness of $h_{min1} \approx 50 - 70$ nm was calculated. In case of the Mobile 1^{TM} ESP Formula 5W-30 and the cast iron wear tests at 80°C a theoretical minimum film thickness of $h_{min2} \approx 6 - 7$ nm was calculated. Within the estimation of the initial λ-ratios (Table 8) only the polished 18CrNiMo7-6 wear test ranged closest to the mixed lubrication regime.

Table 8: Tallian factors

Topography and Material of the Body	Initial Tallian Factor	after 0.6 Mio. cycles	after 2 Mio. cycles
Milled (18CrNiMo7-6)	0.18	0.24	0.23
Polished (18CrNiMo7-6)	0.78	0.38	0.14
Milled (EN-GJS-HB 265)	0.012	0.016	0.028
Polished (EN-GJS-HB 265)	0.056	0.02	0.022

3.5 Specific Dissipated Friction Power (SPFP)

The contact temperature increase calculations render values below 14 K and, therefore, will not be regarded in this paper for further discussions. The SPFP values will be given in W/mm^2 even though the local contact spots are smaller.

---

* Technical contribution to the 2nd International Brazilian Conference on Tribology – TriboBR 2014, November 3rd to 5th, 2014, Foz do Iguaçu, PR, Brazil.

3.5.1 Milled Bodies

a) initial Topography   b) after 2 Mio. cycles
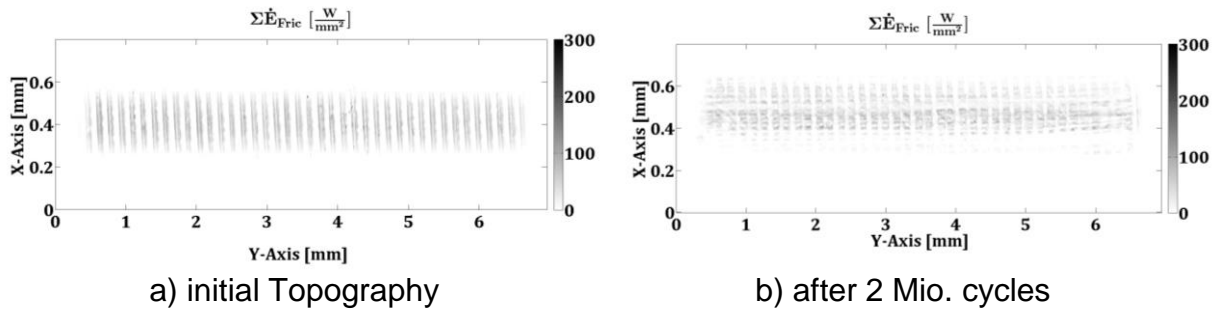
Figure 11. Sum of SPFP and accumulated affected area over SPFP plots of milled 18CrNiMo7-6 wear test

Figure 11 shows the SPFP of the very first (Figure 11a) half cycle of the milled 18CrNiMo7-6 wear tests. Obviously the summits of the machined asperities are in contact while some areas dissipate more friction power than others. This depicts the localized dissipation at the beginning of the run-in process. By integrating over the entire affected contact area the average SPFP value is 29 W/mm^2 with a standard deviation of 25 W/mm^2. This shows that some spots dissipated quite high values of up to 300 W/mm^2, while others don't. After run in (Figure 11b) the topography has changed leveling out the average value to 15 W/mm^2 but still showing a distinct scatter of ±16 W/mm^2. This is also depicted by some spots that still dissipate 300 W/mm^2.

a) initial Topography   b) after 2 Mio. cycles
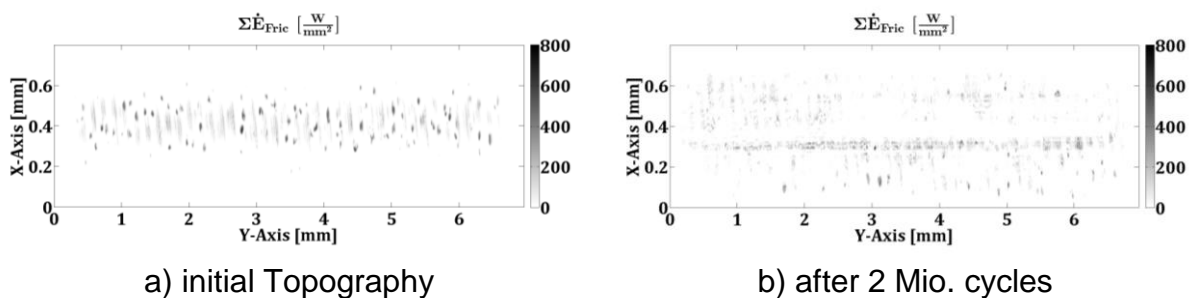
Figure 12. Sum of specific dissipated friction power of milled EN-GJS-HB 265 wear test

For the milled EN-GJS-HB 265 the affected contact area looks different as can be qualitatively concluded from the 2D surface profile in Figure 12a. Due to the smaller affected contact area the maximum values are higher reaching 800 W/mm^2 while the average value is 53±82 W/mm^2 at the beginning of the run-in process. After 2 Mio. cycles (Figure 12b) the average dissipated friction power decreases to 32 W/mm^2 but statistically the scatter remains high at ±52 W/mm^2. Due to the fact that negative friction power is impossible the use of purely statistical methods as proposed earlier [15] remains questionable at this point.

---

* Technical contribution to the 2nd International Brazilian Conference on Tribology – TriboBR 2014, November 3rd to 5th, 2014, Foz do Iguaçu, PR, Brazil.

3.5.1 Polished Bodies

a) initial topography   b) after 2 Mio. cycles
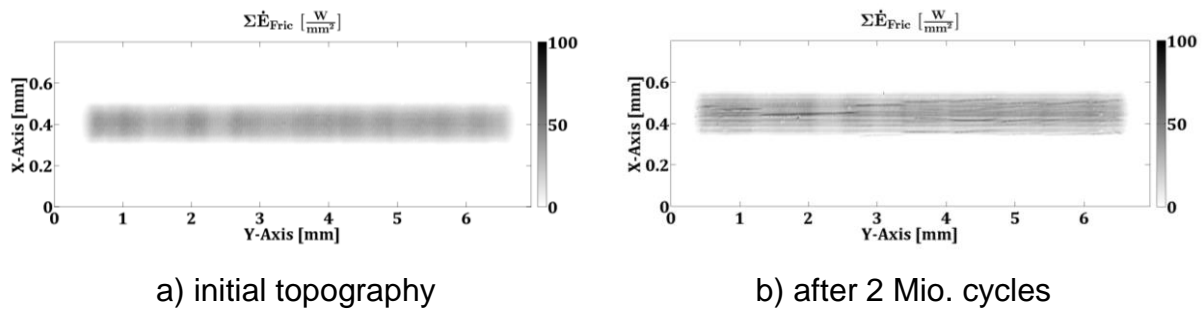
Figure 13. Sum of specific dissipated friction power of polished 18CrNiMo7-6 wear test

Figure 13a shows the SPFP of the polished 18CrNiMo7-6 wear tests. Now the affected area is larger and more homogenously distributed, which qualitatively results in smaller average (21 ± 11 W/mm^2) and peak values already at run-in. Even after 2 Mio. cycles (Figure 13b) the scratches in the direction of the relative velocity do not alter that situation distinctly with 21 ± 15 W/mm^2.

a) initial topography   b) after 2 Mio. cycles
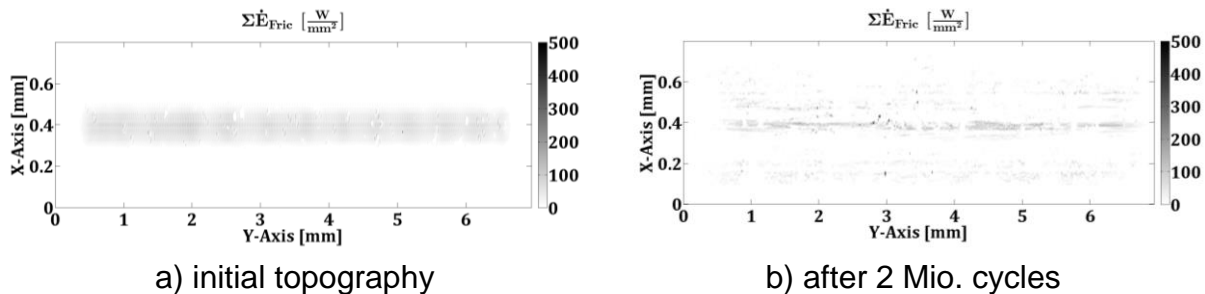
Figure 14. Sum of specific dissipated friction power of polished EN-GJS-HB 265 wear test

Again the polished cast iron EN-GJS-HB 265 behaves differently. At run in (Figure 14a) the affected contact area appears even but the higher coefficient of friction a slightly higher specific dissipated friction power of 30 ± 21 W/mm^2. Now after 2 Mio. cycles (Figure 14b) the contact area is much smaller but the COF decreased distinctly resulting in 11 ± 21 W/mm^2. The extreme scatter can be attributed to those contact spot, which now have to dissipate up to 500 W/mm^2, while the low average value is related to the activation of the graphite as solid lubricant.

4 DISCUSSION

In order to discuss the results of the specific dissipated friction power it should be mentioned that the chosen dimension of W/mm^2 has been chosen for its commonly use. Certainly it should be discussed whether this is useful because the contact spots, which dissipate the power and, therefore, most of the wear loss, are smaller. But the same is true for e.g. wear rates in nm/h, if the numbers become smaller than the size of an atom and the wear particles in a carburized steel vs. hardened steel contact are in the range of about 300 nm [16]. This discrepancy between integrated values and real mechanisms is still matter of research and should not be discussed here. This paper should only give a first insight about an approach into the localized character of boundary lubricated ultra-mild sliding wear in contrast to the well-investigated mild sliding wear of some µm/h. The latter is generated in most standard

---

laboratory tribometers for the sake of testing time and reproducibility even though practical applications would never allow for such high wear rates.

According to the measurements and calculations every part of the affected contact area has to undergo a different tribological load situation over time. Thus one can classify those fractions, which dissipate a certain power, and add them to the other SPFP-groups between the smallest and the largest value. Thus one would see how much energy is dissipated via which contact area. Figure 15 shows such figures for the milled steel and the milled cast iron. From the classical point of view the run-in should start at high friction with a small contact area (lower right corner) and reach smaller friction value with a large contact area within steady state (upper left corner).

a) carburized 18CrNiMo7-6   b) flame hardened EN-GJS-HB 265
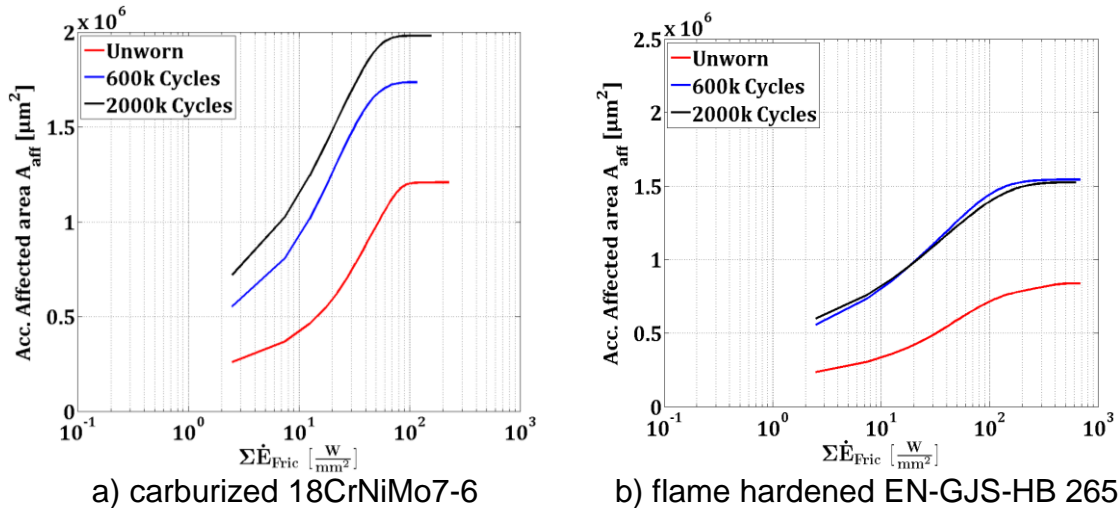
Figure 15. Accumulated Affected Contact Area and Specific Dissipated Friction Power of Milled Surfaces

From Figure 15 a one can see that the steel couple dissipates between 2 and 200 W/mm^2 at the beginning of run-in. It can also be seen that for a certain friction power the area increases with the numbers of cycles and might settle at a steady-state relationship (here assumed at 2 Mio. cycles). As soon as two curves match steady-state would be reached. Thus such diagram gives quantitative values for a visual impression about the tribological loads in the real area of contact. Obviously the cast iron starts at a totally different contact situation leading to a smaller affected area that dissipates higher friction power (Figure 15 b). The power values range from 2 to 800 W/mm^2 and the gradient of the curve is much smaller as for the steel. The steady state is reached already after 600.000 cycles but the affected contact area always remains smaller compared to that of the steel couple. Obviously the graphite protruding to the contact surfaces could not be activated as additional solid lubricant. Thus the milled cast iron-polished 52100 steel contact dissipates more frictional energy per contact area over the entire test period than the milled steel-polished steel couple, which would explain the threefold higher wear rate at about a 20 % higher COF.

For the polished surfaces the picture changes (Figure 16). The polished steel-couple dissipates less friction power already at the beginning of run-in with values between 2 and 40 W/mm^2. After 600.00 only little changes of the topography results in a higher max. value of 60 W/mm^2. The slope of the curve is close to 0 because such highly localized and only a few contact spots do not distinctly add to the increase of the affected contact area. Even after 2 Mio. cycles the changes remain small as to the increase of the contact area as well as to the max. friction power of 100 W/mm^2.

Even though the COF is about the same for the milled and polished couples and the polished one maintains a smaller affected contact area it shows a 28fold smaller wear rate. This gives rise to the assumption that not the entire affected contact area as the entire dissipated friction power result in wear. Maybe it is just the few and localized max. values or those above an unknown critical one that bring about an unstable material reaction and generate a wear particle.

a) carburized 18CrNiMo7-6   b) flame hardened EN-GJS-HB 265
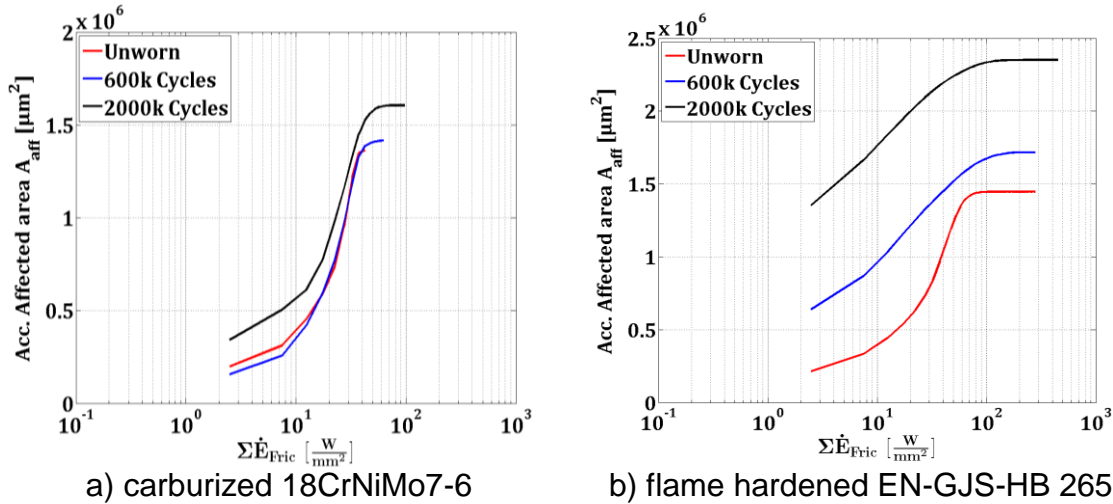
Figure 16. Accumulated Affected Contact Area and Specific Dissipated Friction Power of Polished Surfaces

The steep decrease of the COF for the polished cast iron-polished 52100 couple in figure 4 points on graphite as solid lubricant. Still the dissipated friction power values range from 2 to 300 W/mm^2 because of the smaller affected contact area. After 600.000 cycles the system is still in run-in and after 2. Mio. cycles steady state can just be assumed. Still the affected area becomes distinctly larger with the numbers of cycles which here is mainly attributed to the topography changes of the counter-body. Again the 0-slope of the affected area for the max. values between 100 and 400 W/mm^2 points on the marked localization of the tribological loading. In comparing the milled and the polished cast iron tests it is obvious the threefold decrease of the average dissipated friction power relates better to the 3fold decrease of the wear rate than the 50% decrease of the COF.

Finally the question arises whether tribological systems with similar wear rates under ultra-mild sliding wear can be assumed being similar. In an earlier paper we have shown the energy dissipated per worn volume allows for a qualitative criterion as to the dominating wear mechanisms [17]. From this it followed that a higher value of worn volume per accumulated dissipated friction energy (mm^3/J) points towards more mechanically-dominated wear mechanisms (here surface fatigue) while the opposite would give rise to chemically-dominated ones (here tribochemical reactions). If we apply this to the wear tests in this paper at 2 Mio. cycles both surfaces of the cast iron vs. 52100 couple render with roughly a factor of two: milled 1.68x10^{-8} mm^3/J; polished 2.98x10^{-8} mm^3/J. This marked difference points on a distinct influence of tribochemical reactions on the behavior of the polished couple.

If this is applied for the self-mating steel couple one gets: milled 8.0x10^{-9} mm^3/J; polished 2.7x10^{-10} mm^3/J at about the same COF. Again this marked difference points on a distinct influence of tribochemical reactions on the behavior of the polished couple.

Finally one can derive that in order to wear a certain volume of such steel couple with a milled vs. polished surface one needs about twice as much energy compared to milled cast iron vs. polished 52100, while for the polished surfaces one would need about a 110fold higher friction energy.

5 CONCLUSIONS

In this study a combined experimental and numerical experiments were conducted for a carburized self-mating 18CrNiMo7-6 couple and flame hardened EN-GJS-HB 265 vs. 52100 steel couple. The measured values were shown and discussed in relation to the affected contact A_{aff} and the specific dissipated friction power ΣE_{Fric}. This brought about the following results:

The relation between A_{aff} and ΣE_{Fric} alters between run-in and steady state but does not follow the simple assumption that A_{aff} increases over time while ΣE_{Fric} decreases.

Neither standardized surface parameters nor the COF render sufficient information about the tribological performance.

By using A_{aff} and ΣE_{Fric} one can evaluate the contact in more detail as to the localization of the highly loaded contact areas. This allows for a better understanding of the influence of the topography and its changes on ultra-mild sliding wear.

In order to further improve the information from such evaluation it has to be carried out separately for body and counter-body.

In addition there is a need for the knowledge under which dissipated friction power values the material is unaffected (e.g. $\Sigma E_{Fric,0}$) and above which it would become instable (e.g. $\Sigma E_{Fric,c}$). These values are not known at this point.

Finally these criteria have to be connected to the local stress-state, which will be investigated in the future.

Acknowledgments

REFERENCES

1   Archard, J.F., Contact and rubbing of flat surfaces. Journal of Applied Physics, 1953. 24(8): p. 981-988.
2   Dienwiebel, M. and M. Scherge, Nanotribology in Automotive Industry, in Fundamental of Friction and Wear on the Nanoscale, E. Gnecco and E. Meyer, Editors. 2007, Springer. p. 548 - 560.
3   Summer-Smith, J.D., An Introductory Guide to Industrial Tribology. 1994, London, UK: Mechanical Engineering Publications Limited.
4   Polonsky, I.A. and L.M. Keer, A numerical method for solving rough contact problems based on the multi-level multi-summation and conjugate gradient techniques. Wear, 1999. 231: p. 206 - 219
5   Ungureanu, I. and S. Spinu, A simplified model for pressure distribution in elastic - perfectly plastic contact. ANNALS of the Oradea University, 2010. IX: p.1-8.
6   Ruge, J. and H. Wohlfahrt, Technologie der Werkstoffe. 8 ed. 2007: Vieweg.
7   Goeke, S., et al., Enhancing the Surface Integrity of Tribologically Stressed Contacting Surfaces by an Adjusted Surface Topography. Proceedia CIRP, 2014: p. 1-5.

8   Chittenden, R.J., et al., A theoretical analysis of the isothermal elastohydrodynamic lubrication of concentrated contacts: I. Direction of lubricant entrainment coincident with the major axis of the Hertzian contact ellipse. Proceeding of the Royal Society of London, 1984. 97(A): p. 245 - 269.

9   Liu, S. and Q. Wang, Studying Contact Stress Fields Caused by Surface Tractions With a Discrete Convolution and Fast Fourier Transform Algorithm. Journal of Tribology, 2002. 124: p. 36 - 45.

10   Liu, S., Q. Wang, and G. Liu, A versatile method of discrete convolution and FFT (DC-FFT) for contact analyses. Wear, 2000. 243: p. 101-111.

11   Jacq, C., et al., Development of a Three-Dimensional Semi-Analytical Elastic-Plastic Contact Code. ASME Journal of Tribology, 2001. 124: p. 653-667.

12   Tallian, T.E., On competing failure modes in rolling contact. ASLE Transactions, 1967. 10: p. 418 - 439.

13   Willner, K., Fully Coupled Frictional Contact Using Elastic Halfspace Theory. ASME Journal of Tribology, 2008. 130: p. 1 -8.

14   GfT, Arbeitsblatt 7: Tribologie, in Verschleiß, Reibung2002, Gesellschaft für Tribologie e.V.: Aachen, Germany

15   Stickel, D. and A. Fischer, The Alteration of Micro-Contact Parameters during Run-In and their Effect on the Specific Dissipated Friction Power. Tribol. Int., 2014: p. accepted.

16   Samerski, I., et al., The transition between high and low wear regimes under multidirectional reciprocating sliding. Wear, 2009. 267(9-10): p. 1446-1451.

17   Hanke, S., et al., The role of wear particles under multidirectional sliding wear. Wear, 2009. 267(5-8): p. 1319-1324.